

Perfect kagome-lattice antiferromagnets with $J_{\text{eff}} = 1/2$: The Co^{2+} -analogs of copper minerals volborthite and vesignieite

Yuya Haraguchi^{1,†}, Takehiro Ohnoda¹, Akira Matsuo², Koichi Kindo², and Hiroko Aruga Katori¹

¹Department of Applied Physics and Chemical Engineering, Tokyo University of Agriculture and Technology, Koganei, Tokyo 184-8588, Japan

²The Institute for Solid State Physics, The University of Tokyo, Kashiwa, Chiba 277-8581, Japan

†chiyuya3@go.tuat.ac.jp

We report the synthesis, crystal structure, and magnetic properties of Co^{2+} kagome magnets $\text{Co}_3\text{V}_2\text{O}_7(\text{OH})_2 \cdot 2\text{H}_2\text{O}$ and $\text{BaCo}_3(\text{VO}_4)_2(\text{OH})_2$, which can be recognized as Co-analogues of the intensively researched quantum kagome magnet volborthite $\text{Cu}_3\text{V}_2\text{O}_7(\text{OH})_2 \cdot 2\text{H}_2\text{O}$ and vesignieite $\text{BaCu}_3(\text{VO}_4)_2(\text{OH})_2$. For each compound, the ground state is seemingly A-type antiferromagnetic order. At low temperatures, applying a magnetic field causes a metamagnetic-like transition described by the transition in which antiferromagnetically-aligned canted moments change to ferromagnetically-aligned ones. These ground and field-induced states include a canted ferromagnetic component perpendicular to the kagome planes favored by Dzyaloshinskii-Moriya interactions. These magnetic properties are well characterized by the $J_{\text{eff}} = 1/2$ physics. Our findings will be the first step toward clarifying the $J_{\text{eff}} = 1/2$ kagome physics, which has been little studied experimentally or theoretically.

I. Introduction

Spin-1/2 kagome-lattice antiferromagnets (KAFMs) are one of the most promising spin models to realize a highly entangled quantum spin-liquid (QSL) ground state [1-4]. However, the realistic KAFM materials deviate from the ideal model due to various intertwined perturbations. For example, in herbertsmithite $\text{ZnCu}_3(\text{OH})_6\text{Cl}_2$, the "gold standard" in the KAFM exhibiting QSL behavior [5,6], the local spin correlations are greatly perturbed by chemical disorder, the nature of which has not yet been revealed [7-10]. It is also predicted that chemical perturbations will mimic QSL-like behavior [11,12]. Thus, it is crucial to deeply understand the individual roles of perturbations that will always be included in realistic materials. Under this circumstance, the development of new kagome-lattice materials is desirable.

The number of ions that can realize the $S = 1/2$ state, which can form the kagome-lattice, is minimal. Among them, physicists and material scientists have successively found promising compounds in the mineral database that constitute the kagome-lattice composed of Cu^{2+} ions. Thus, synthetic copper minerals have been the mainstream in quantum frustrated magnetism research. Examples include herbertsmithite, volborthite $\text{Cu}_3\text{V}_2\text{O}_7(\text{OH})_2 \cdot 2\text{H}_2\text{O}$ [13-15], vesignieite $\text{BaCu}_3(\text{VO}_4)_2(\text{OH})_2$ [16], and Cd-kapellasite $\text{CdCu}_3(\text{OH})_6(\text{NO}_3)_2 \cdot \text{H}_2\text{O}$ [17,18]. However, Cu^{2+} ions are highly susceptible to symmetry breaking because of their intense Jahn-Teller activity. Therefore, they tend to deviate

from the ideal kagome model. On the other hand, Ti^{3+} ions can also realize $S = 1/2$, and their Jahn-Teller activity is not as

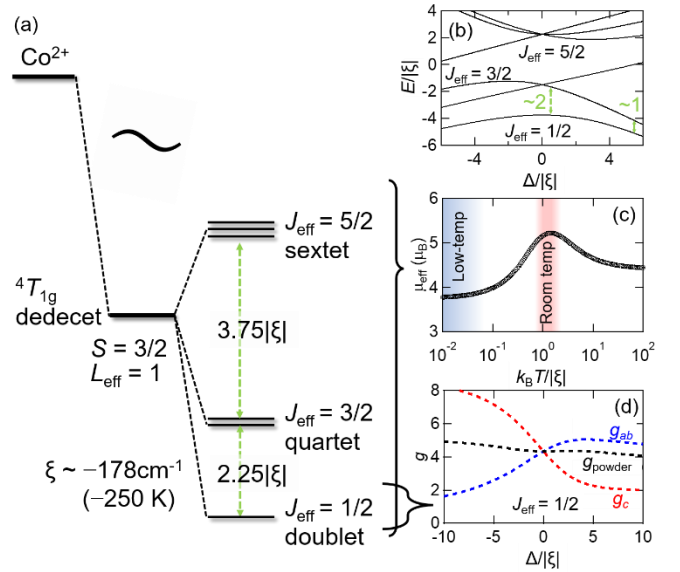


Fig. 1 (a) Energy levels scheme of high-spin d^7 ion under octahedral crystal field and spin-orbit coupling and (b) their trigonal crystal field Δ derivative. (c) The theoretical effective magnetic moment μ_{eff} as a function of $k_B T/|\xi|$ in Co^{2+} ion with octahedral crystal fields, where k_B is the Boltzmann constant. (d) The anisotropic and powder-averaged g factors in Co^{2+} ion as a function of $\Delta/|\xi|$.

significant as that of Cu^{2+} ions, so there is a possibility that an ideal kagome model with minor perturbation can be realized. However, all the Ti^{3+} KAFMs reported so far are strongly distorted, resulting in a significant deviation from the kagome model [19,20].

We focus on Co^{2+} as a new candidate ion for achieving a spin-1/2 state. The single-ion magnetic property of Co^{2+} in an octahedral environment is determined by the 12-fold degenerated (dodecet) ground state manifold $^4T_{1g}$ [21-23]. Due to spin-orbit coupling, this dodecet splits into three manifolds—doublet, quartet, and sextet, as shown in Fig. 1(a). The lowest-energy state is given by $J_{\text{eff}} = 1/2$ Kramers doublet. As shown in Fig. 1(b), $J_{\text{eff}} = 1/2$ is always the lowest energy regardless of the trigonal distortion, and the energy gap from the excited state is approximately $|\xi|$ to $2|\xi|$. Therefore, if the temperature is a much smaller energy scale than the spin-orbit interaction $\xi = -178 \text{ cm}^{-1}$ ($\sim -250 \text{ K}$), the magnetic properties are governed by the lowest energy $J_{\text{eff}} = 1/2$ Kramers doublet.

Therefore, treating Co^{2+} compounds as a $J_{\text{eff}} = 1/2$ doublet physics is possible in the low-temperature region. However, physicists must pay carefulness to the temperature dependence in the physical properties. The contribution of the excited states, $J_{\text{eff}} = 3/2$ quartet and $J_{\text{eff}} = 5/2$ sextet, by the Boltzmann distribution must cause the effective magnetic moment to change with temperature. Figure 1(c) shows the theoretically-calculated μ_{eff} for non-interacting Co^{2+} in an octahedral crystal field with spin-orbit couplings $H = \xi L \cdot S$, and L is the total orbital quantum number [24]. It is written as

$$\mu_{\text{eff}}(\text{Co}^{2+}) = \sqrt{\frac{3\left\{\frac{63x}{20} + \frac{98}{25} + \left(\frac{640x}{225} + \frac{4312}{2025}\right)e^{-\frac{15x}{4}} + \left(\frac{169x}{36} - \frac{490}{81}\right)e^{-6x}\right\}}{x\left\{3 + 2e^{-\frac{15x}{4}} + e^{-6x}\right\}}} \quad (1)$$

, where $x = \xi/k_{\text{B}}T$. This theoretical calculation yields $\mu_{\text{eff}} \sim 5.2 \mu_{\text{B}}$ near room temperature and $\sim 4 \mu_{\text{B}}$ at low temperatures. Conversely, detecting the temperature variation of μ_{eff} makes it possible to demonstrate a realization of $J_{\text{eff}} = 1/2$ physics in realistic Co^{2+} materials at low temperatures.

In addition, physicists should also pay carefulness to the effects of low-symmetry crystal fields when considering only the $J_{\text{eff}} = 1/2$ doublet at low temperatures. In a perfect octahedral crystal field, there is no anisotropy in the Zeeman splitting of the doublet in a magnetic field. On the other hand, in an axis-symmetric crystal field such as a trigonal or tetragonal crystal field, there is a change in energy between the case parallel to the c -axis and the case perpendicular to it. Therefore, anisotropy appears in the g -value. Figure 1(d) shows the g -values expressed as a function of the parameter $\Delta/|\xi|$, where Δ is the trigonal distortion energy [22,25]. Here, $\Delta/|\xi| < 0$ means trigonally-elongated the CoO_6 octahedron along the c -axis and $\Delta/|\xi| > 0$ trigonally-compressed. The powder-averaged $g_{\text{powder}} = [(2g_{\text{ab}}^2 + g_{\text{c}}^2)/3]^{0.5}$ of the powder sample is almost unchanged and is approximate $g_{\text{powder}} \sim 4$, although there is a slight Δ dependence. Therefore, the experimental observation of a powder-averaged g -value close to 4 at low temperatures in the powder sample is a criterion for satisfying the $J_{\text{eff}} = 1/2$ condition.

Unlike Cu^{2+} or Ti^{3+} KAFMs, there is a limited number of

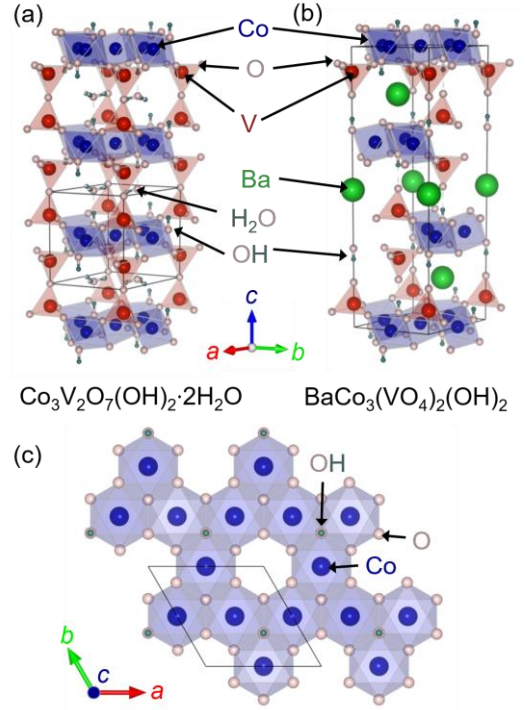


Fig. 2 Crystal structures of (a) $\text{Co}_3\text{V}_2\text{O}_7(\text{OH})_2 \cdot 2\text{H}_2\text{O}$ and (b) $\text{BaCo}_3(\text{VO}_4)_2(\text{OH})_2$ viewed along the c axis. (c) The $\text{Co}_3\text{O}_6(\text{OH})_2$ kagome layer viewed along the ab plane commonly observed in $\text{Co}_3\text{V}_2\text{O}_7(\text{OH})_2 \cdot 2\text{H}_2\text{O}$ and $\text{BaCo}_3(\text{VO}_4)_2(\text{OH})_2$. The VESTA program is used for visualization [31].

candidates for the Co^{2+} KAFMs, so experimental studies have been limited. $\text{Co}_3\text{Mg}(\text{OH})_6\text{Cl}_2$ contains $\sim 7\%$ site-mixture between the Mg^{2+} and Co^{2+} sites, resulting in a spin glass character due to randomness [26]. Moreover, synthesis of $\text{BaCo}_3(\text{VO}_4)_2(\text{OH})_2$ [27] and $\text{Co}_3\text{V}_2\text{O}_7(\text{OH})_2 \cdot 2\text{H}_2\text{O}$ [28], Co^{2+} -analogues of vesignieite and volborthite, have also been reported. Their crystal structures are shown in Figs. 2(a) and 2(b). Both compounds commonly comprised $\text{Co}_3\text{O}_6(\text{OH})_2$ kagome layer [Figs. 2(c)]. Both compounds exhibit superparamagnetism without magnetic orderings, probably due to finite-size effects [29,30].

This work reports the successful synthesis of high-quality $\text{Co}_3\text{V}_2\text{O}_7(\text{OH})_2 \cdot 2\text{H}_2\text{O}$ and $\text{BaCo}_3(\text{VO}_4)_2(\text{OH})_2$ polycrystalline samples, as well as their magnetic properties. The crystal structure analysis demonstrates the formation of a perfect kagome-lattice without distortion and site mixture. Moreover, the magnetic and thermodynamic properties commonly observed in both materials are well characterized in the $J_{\text{eff}} = 1/2$ state. Our findings demonstrate that $\text{Co}_3\text{V}_2\text{O}_7(\text{OH})_2 \cdot 2\text{H}_2\text{O}$ and $\text{BaCo}_3(\text{VO}_4)_2(\text{OH})_2$ are promising model compounds $J_{\text{eff}} = 1/2$ KAFMs.

II. Experimental Methods

Polycrystalline samples were prepared using the hydrothermal method. All starting materials were purchased from FUJIFILM Wako Pure Chemical Corporation. For

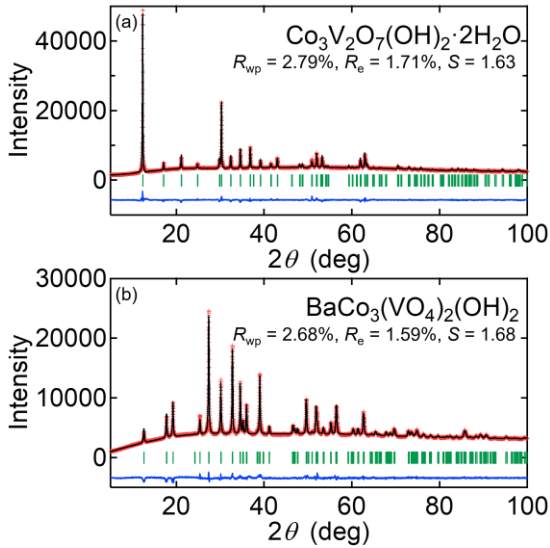


Fig. 3 (a) Powder x-ray diffraction patterns of (a) $\text{Co}_3\text{V}_2\text{O}_7(\text{OH})_2 \cdot 2\text{H}_2\text{O}$ and (b) $\text{BaCo}_3(\text{VO}_4)_2(\text{OH})_2$. The observed intensities (red), calculated intensities (black), and their differences (blue) are shown. Green vertical bars indicate the positions of Bragg reflections.

$\text{Co}_3\text{V}_2\text{O}_7(\text{OH})_2 \cdot 2\text{H}_2\text{O}$, a Teflon beaker containing 0.37g of $\text{Co}(\text{NO}_3)_2 \cdot 6(\text{H}_2\text{O})$, 0.1 g of NH_4VO_3 , 0.07 g of NaOH , and 10 ml of pure H_2O , was heated at 120°C for 60 h. For $\text{BaCo}_3(\text{VO}_4)_2(\text{OH})_2$, a Teflon beaker of 30 ml volume containing 0.35 g of $\text{Ba}(\text{OH})_2 \cdot 8\text{H}_2\text{O}$, 0.78 g of $\text{CoCl}_2 \cdot 2\text{H}_2\text{O}$, 0.14 g of NH_4VO_3 , and 5 ml of pure H_2O , was heated at 200°C for 12 h. In both syntheses, orange-colored powders were obtained after rinsing with distilled water several times and drying at 110°C . The thus-obtained samples were characterized by powder x-ray diffraction (XRD) using $\text{Cu-K}\alpha$ radiation. The cell parameters and crystal structure were refined by the Rietveld method using the RIETAN-FP version 2.16 software [32]. The temperature dependence of magnetization was measured under magnetic fields up to 7 T in a magnetic property measurement system (MPMS; Quantum Design). The temperature dependence of heat capacity was measured by a conventional relaxation method in a physical property measurement system (PPMS; Quantum Design). Magnetization curves up to approximately 50 T were measured by the induction method in a multilayer pulsed magnet at the International Mega Gauss Science Laboratory in Institute for Solid State Physics.

III. Results

A. Crystal structures

Figures 3(a) and (b) show the powder XRD pattern of $\text{Co}_3\text{V}_2\text{O}_7(\text{OH})_2 \cdot 2\text{H}_2\text{O}$ and $\text{BaCo}_3(\text{VO}_4)_2(\text{OH})_2$. For both samples, the observed XRD patterns are perfectly reproduced well using previously-reported crystal structure parameters without changing any parameters, confirming that our samples are single-phase and match the trigonal structures. The crystal structure commonly in $\text{Co}_3\text{V}_2\text{O}_7(\text{OH})_2 \cdot 2\text{H}_2\text{O}$ and

$\text{BaCo}_3(\text{VO}_4)_2(\text{OH})_2$ contains an edge-sharing network of CoO_6 octahedra as shown in Fig. 2(c), where the Co atoms form a perfect kagome-lattice. There is only-one crystallographic Co site and Co-Co distance in the kagome-lattice. Each Co ion is surrounded by six anions: two OH ions and four O ions. The bonds are short for the OH ions at the trans position, and long for the four lateral O ions. The 2-short-4-long-type crystal field must affect the single-ion anisotropy in the $J_{\text{eff}} = 1/2$ pseudospin of Co^{2+} .

B. Magnetic Property

Figures 4(a) and (b) show the temperature dependencies of magnetic susceptibility χ and their inverse $1/\chi$ for $\text{Co}_3\text{V}_2\text{O}_7(\text{OH})_2 \cdot 2\text{H}_2\text{O}$ and $\text{BaCo}_3(\text{VO}_4)_2(\text{OH})_2$. In the $1/\chi$ curves, a slope change is observed around 50 K. The effective magnetic moments μ_{eff} and Weiss temperature θ_{W} obtained by the Curie-Weiss (CW) fits of the $1/\chi$ curves in high-temperatures (150-300 K) and low-temperatures (10-25 K) are listed in the Table 1. In common with both materials, the μ_{eff} values are $\sim 5.2 \mu_{\text{B}}$ for high-temperature regions and $\sim 4.2 \mu_{\text{B}}$ for low-temperature regions, which is roughly consistent with the theoretical calculation shown in Fig. 1(c). Thus, the μ_{eff} -shrinkage is explained in terms of level split owing to spin-orbit couplings. These negative Weiss temperatures indicate that the interaction between Co^{2+} spins is predominantly antiferromagnetic. Furthermore, the change in slope of $1/\chi$ as a function of temperature is observed. For Co^{2+} ions in an octahedral environment, the spacings of the multiplet levels ($J = 1/2, 3/2, \text{ and } 5/2$) are not so large compared to $k_{\text{B}}T$. Thus, the observation of μ_{eff} -decreasing demonstrates a crossover of the multiplet levels.

In both materials, the χ -data increases and then tends to saturate at low temperatures, a characteristic of ferromagnets. On the contrary, as shown in Figure 4(c), the χ -data of $\text{Co}_3\text{V}_2\text{O}_7(\text{OH})_2 \cdot 2\text{H}_2\text{O}$ and $\text{BaCo}_3(\text{VO}_4)_2(\text{OH})_2$ under lower applied fields (10 mT) exhibit antiferromagnetic-like magnetic anomalies at $T_{\text{N}} = 2.7$ and 4.9 K, respectively. A clear magnetic order appeared in these materials, whereas no magnetic order was found in previous reports [29,30], probably due to improved crystallinity and sample quality. In addition, the slight separation of the zero-field cooling (ZFC) and field cooling (FC) curves below T_{N} suggests an emergent magnetic ordering. Figure 4(d) shows the isothermal magnetizations M and their derivative dM/dH at 2 K for $\text{Co}_3\text{V}_2\text{O}_7(\text{OH})_2 \cdot 2\text{H}_2\text{O}$ and $\text{BaCo}_3(\text{VO}_4)_2(\text{OH})_2$. The peaks in the dM/dH data at 75 mT for $\text{Co}_3\text{V}_2\text{O}_7(\text{OH})_2 \cdot 2\text{H}_2\text{O}$ and $\mu_0 H_{\text{M}} = 16$ mT for $\text{BaCo}_3(\text{VO}_4)_2(\text{OH})_2$ indicate a magnetic field-induced phase transition. The M^2 vs. H/M plot [the inset of Fig 4(e)] shows an "S" like behavior because of first-order

Table 1 Experimentally obtained Curie-Weiss parameters at high- (150-300 K) and low-temperatures (10-25 K) in $\text{Co}_3\text{V}_2\text{O}_7(\text{OH})_2 \cdot 2\text{H}_2\text{O}$ and $\text{BaCo}_3(\text{VO}_4)_2(\text{OH})_2$.

Formula	150-300 K		10-25 K	
	μ_{eff} (μ_{B})	θ_{W} (K)	μ_{eff} (μ_{B})	θ_{W} (K)
$\text{Co}_3\text{V}_2\text{O}_7(\text{OH})_2 \cdot 2\text{H}_2\text{O}$	5.138(3)	-17.4(3)	4.49(3)	3.6(1)
$\text{BaCo}_3(\text{VO}_4)_2(\text{OH})_2$	5.087(2)	-22.7(2)	4.25(5)	1.6(1)

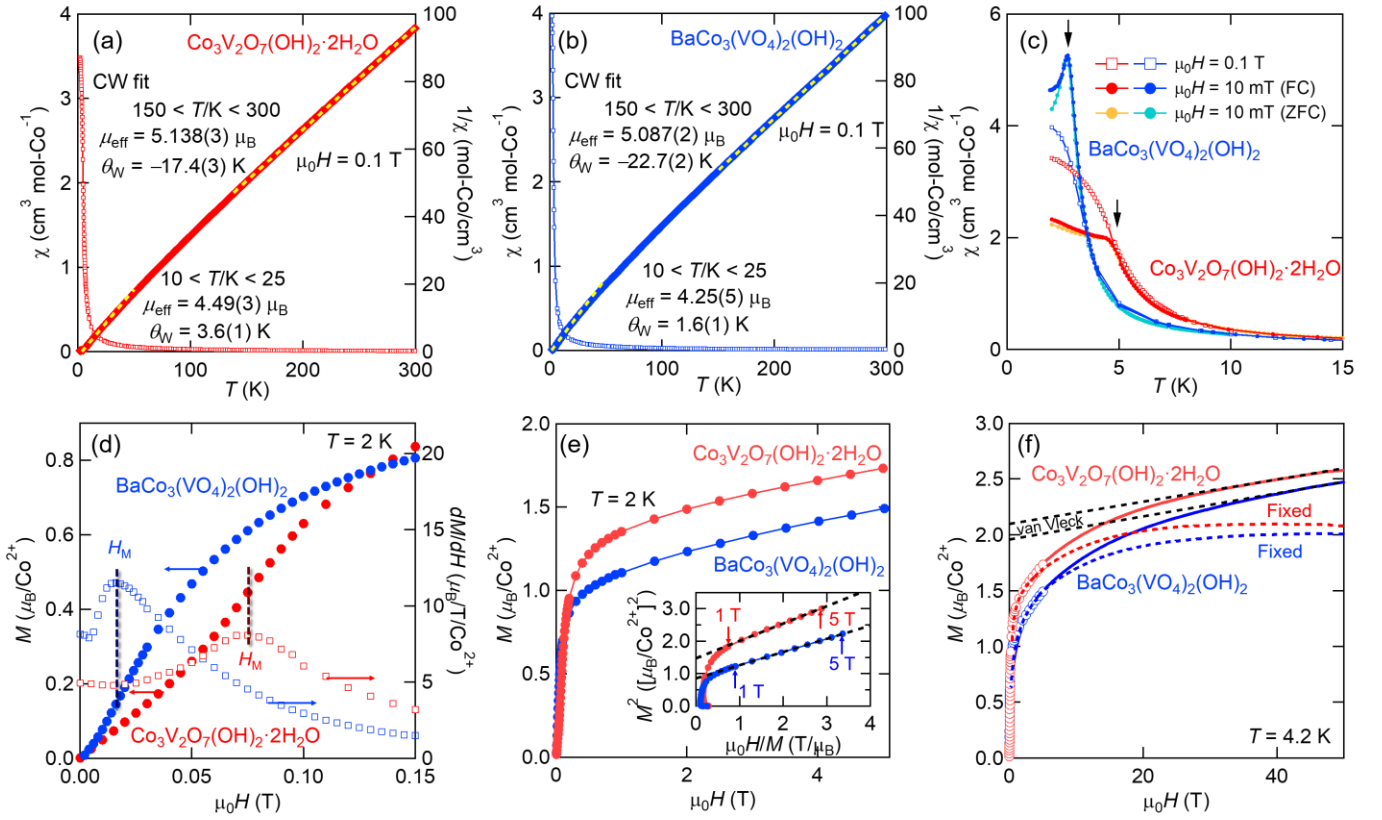


Fig. 4 Temperature dependence of the magnetic susceptibility χ (open symbols) and inverse magnetic susceptibility $1/\chi$ (closed symbols) for (a) $\text{Co}_3\text{V}_2\text{O}_7(\text{OH})_2 \cdot 2\text{H}_2\text{O}$ and (b) $\text{BaCo}_3(\text{VO}_4)_2(\text{OH})_2$. The dotted lines on the $1/\chi$ data represent fits to the Curie-Weiss (CW) model at high- ($150 < T/\text{K}$) and low-temperature ($10 < T/\text{K} < 25$) regions. (c) Temperature dependences of χ measured for magnetic fields of 0.1 T and 10 mT. (d) Low field (< 0.15 T) magnetization curves M and their derivative dM/dH measured at 2 K for $\text{Co}_3\text{V}_2\text{O}_7(\text{OH})_2 \cdot 2\text{H}_2\text{O}$ and $\text{BaCo}_3(\text{VO}_4)_2(\text{OH})_2$. The metamagnetic-like transition is observed at $\mu_0 H_M = 75$ mT for $\text{Co}_3\text{V}_2\text{O}_7(\text{OH})_2 \cdot 2\text{H}_2\text{O}$ and $\mu_0 H_M = 16$ mT for $\text{BaCo}_3(\text{VO}_4)_2(\text{OH})_2$. (e) The M data at 2 K up to 5 T for $\text{Co}_3\text{V}_2\text{O}_7(\text{OH})_2 \cdot 2\text{H}_2\text{O}$ and $\text{BaCo}_3(\text{VO}_4)_2(\text{OH})_2$. The inset shows the M^2 vs $\mu_0 H/M$ plot. (f) Magnetization curves M measured at 4.2 K under pulsed magnetic fields up to 50 T for $\text{Co}_3\text{V}_2\text{O}_7(\text{OH})_2 \cdot 2\text{H}_2\text{O}$ and $\text{BaCo}_3(\text{VO}_4)_2(\text{OH})_2$. The magnitudes are calibrated to the data measured under static fields up to 5 T (open circles).

metamagnetic transition according to Landau theory [33]. Also, metamagnetism is universally observed in A-type antiferromagnets with intralayer-ferromagnetically-coupled layers [34–38]. The origin of the A-type-antiferromagnetic-ferromagnetic phase transition at low magnetic fields appears to be due to weak interlayer coupling. Therefore, we conclude that the title materials are A-type antiferromagnets.

The good linearity of the M^2 vs. H/M plot with a positive value intercept in the 1 ~ 5 T field region indicates that the spontaneous magnetization M_0 in the category of Landau theory is an order parameter in the field-induced phase [39]. The M_0 values obtained as the intercept of the linear fit are $M_0 = 1.21 \mu_B$ for $\text{Co}_3\text{V}_2\text{O}_7(\text{OH})_2 \cdot 2\text{H}_2\text{O}$ and $M_0 = 0.924 \mu_B$ for $\text{BaCo}_3(\text{VO}_4)_2(\text{OH})_2$. In general, the ground state of Co^{2+} is well described by $J_{\text{eff}} = 1/2$ pseudospin as shown in Fig. 1(a), and the powder-averaged g -factor is ~ 4 [see Fig. 1(d)]; thus, $M_{\text{sat}} \sim 2\mu_B$. Compared to M_{sat} , the observed M_0 is relatively small. Figure 4(f) shows the isothermal magnetizations of $\text{Co}_3\text{V}_2\text{O}_7(\text{OH})_2 \cdot 2\text{H}_2\text{O}$ and $\text{BaCo}_3(\text{VO}_4)_2(\text{OH})_2$ up to 50 T. Above 40 T, the M data increase almost linearly due to the large temperature-independent van Vleck paramagnetism of octahedrally-coordinated Co^{2+} ions. Linear fits the M data

above 40 T yield the van Vleck paramagnetic susceptibility χ_{vv} is $5.57 \times 10^{-3} \text{ cm}^3/\text{mol-Co}^{2+}$ for $\text{Co}_3\text{V}_2\text{O}_7(\text{OH})_2 \cdot 2\text{H}_2\text{O}$ and $5.59 \times 10^{-3} \text{ cm}^3/\text{mol-Co}^{2+}$ for $\text{BaCo}_3(\text{VO}_4)_2(\text{OH})_2$. Then, the saturation magnetizations M_{sat} were obtained as $M_{\text{sat}} = 2.10 \mu_B/\text{Co}^{2+}$ for $\text{Co}_3\text{V}_2\text{O}_7(\text{OH})_2 \cdot 2\text{H}_2\text{O}$ and $M_{\text{sat}} = 1.98 \mu_B/\text{Co}^{2+}$ for $\text{BaCo}_3(\text{VO}_4)_2(\text{OH})_2$. Thus, the observed M_{sat} value provides strong evidence that $J_{\text{eff}} = 1/2$ ground state is realized in these materials, yielding the respective powder average g -values as follows: $g = 4.20$ in $\text{Co}_3\text{V}_2\text{O}_7(\text{OH})_2 \cdot 2\text{H}_2\text{O}$ and $g = 3.96$ in $\text{BaCo}_3(\text{VO}_4)_2(\text{OH})_2$. The observation of $M_{\text{sat}} \sim 2$ demonstrates that the reduced M_0 is not due to temperature effects but rather due to the presence of a field-induced phase with a small spontaneous magnetization.

C. Thermodynamic property

Figure 5(a) shows the temperature dependence of the heat capacity divided by temperature C/T of $\text{Co}_3\text{V}_2\text{O}_7(\text{OH})_2 \cdot 2\text{H}_2\text{O}$ and $\text{BaCo}_3(\text{VO}_4)_2(\text{OH})_2$. Clear λ -shaped peaks are observed at 4.6 and 2.7 K for $\text{Co}_3\text{V}_2\text{O}_7(\text{OH})_2 \cdot 2\text{H}_2\text{O}$ and $\text{BaCo}_3(\text{VO}_4)_2(\text{OH})_2$, respectively. Therefore, both in $\text{Co}_3\text{V}_2\text{O}_7(\text{OH})_2 \cdot 2\text{H}_2\text{O}$ and $\text{BaCo}_3(\text{VO}_4)_2(\text{OH})_2$, second-order

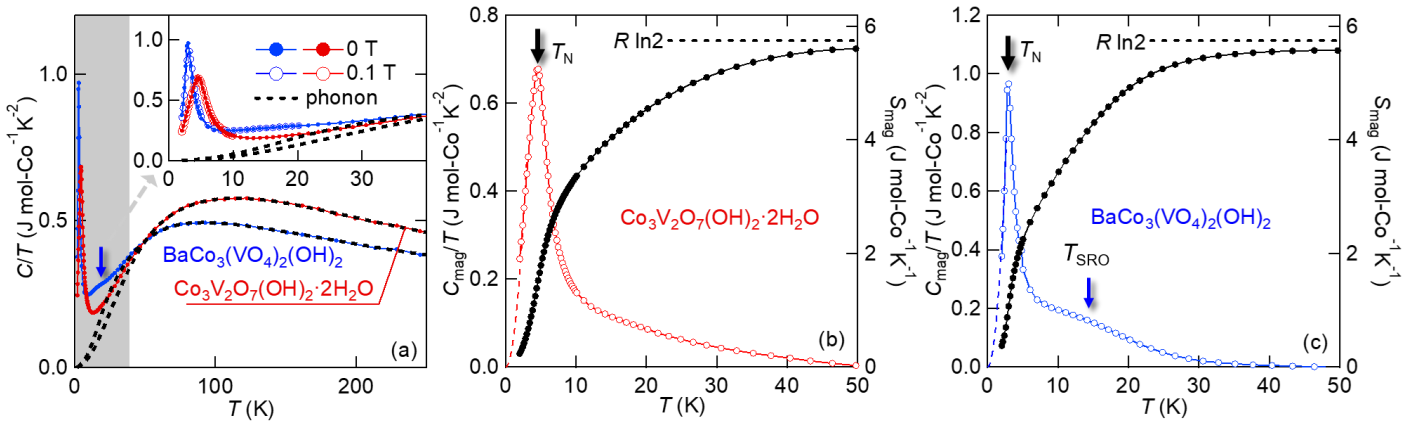


Fig. 5 (a) The total heat capacities divided by temperature C/T of $\text{Co}_3\text{V}_2\text{O}_7(\text{OH})_2 \cdot 2\text{H}_2\text{O}$ and $\text{BaCo}_3(\text{VO}_4)_2(\text{OH})_2$. The inset shows the enlarged view of shaded area. The C/T data with 0.1 T magnetic field applied is also shown as open circles. The dashed lines on the data represent the lattice contribution estimated by fitting the data above 100 K, as described in the text. The temperature dependences of the magnetic heat capacity divided by temperature C_{mag}/T after the subtraction of lattice contribution and magnetic entropy S_{mag} for (b) $\text{Co}_3\text{V}_2\text{O}_7(\text{OH})_2 \cdot 2\text{H}_2\text{O}$ and (c) $\text{BaCo}_3(\text{VO}_4)_2(\text{OH})_2$. The horizontal dashed lines indicate the value of $S_{\text{mag}} = R \ln 2$, which is the total magnetic entropy derived from $J_{\text{eff}} = 1/2$.

magnetic phase transitions with bulk nature occur at T_N . As shown in the inset, even at 0.1 T, where the magnetic anomaly seems to disappear in the magnetic susceptibility, a λ -type peak is almost unchanged. This fact indicates that the magnetic field region above H_M is a robust magnetically ordered state different from the ground state, contrasting with a polarized phase.

Generally, to evaluate the magnetic contribution, the heat capacity of the nonmagnetic analog is used to determine their lattice contributions. Unfortunately, the nonmagnetic counterpart $\text{BaZn}_3(\text{VO}_4)_2(\text{OH})_2$ is unavailable, and the C/T data of $\text{Zn}_3\text{V}_2\text{O}_7(\text{OH})_2 \cdot 2\text{H}_2\text{O}$ (as a natural mineral martyrite [40]) does not match the high-temperature C/T data of $\text{Co}_3\text{V}_2\text{O}_7(\text{OH})_2 \cdot 2\text{H}_2\text{O}$ at all (see the Supplemental Material [41]). Thus, to extract the magnetic contribution to the heat capacity, the lattice contribution was estimated by fitting the high-temperature part where the magnetic heat capacity may be negligible. It is well known that a lattice heat capacity C_{lat} consists of contributions from three acoustic phonon branches and $3n-3$ optical phonon branches, where n is the number of atoms per formula unit [42]; n equals 22 for $\text{Co}_3\text{V}_2\text{O}_7(\text{OH})_2 \cdot 2\text{H}_2\text{O}$ and 18 for $\text{BaCo}_3(\text{VO}_4)_2(\text{OH})_2$. The acoustic and optical contributions are described by the Debye- and Einstein-type heat capacities C_D and C_E , respectively. Provided that C_{lat} is the sum of C_D and C_E , the C/T data above 100 K, where the magnetic heat capacity may be negligible, are fitted to the equation,

$$\begin{aligned}
 C_{\text{lattice}} &= C_D + C_E \\
 &= 9R(T/\theta_D)^3 \int_0^{\theta_D/T} \frac{x^4 \exp(x)}{[\exp(x) - 1]^2} dx \\
 &\quad + R \sum_{i=1}^3 n_i \frac{(\theta_{Ei}/T)^2 \exp(\frac{\theta_{Ei}}{T} - 1)}{\exp(\frac{\theta_{Ei}}{T} - 1)} \quad (4)
 \end{aligned}$$

, where R is the gas constant, θ_D is the Debye temperature, θ_{Ei} is the Einstein temperatures. The best fits are shown by the dashed lines with $\theta_D = 180(2)$ K, $\theta_{E1} = 260(9)$ K, $\theta_{E2} = 552(12)$ K, $\theta_{E3} = 1677(24)$ K, $n_1 = 17$, $n_2 = 23$, and $n_3 = 23$ for $\text{Co}_3\text{V}_2\text{O}_7(\text{OH})_2 \cdot 2\text{H}_2\text{O}$ and $\theta_D = 153(4)$ K, $\theta_{E1} = 227(9)$ K, $\theta_{E2} = 633(11)$ K, $\theta_{E3} = 1544(52)$ K, $n_1 = 16$, $n_2 = 17$, and $n_3 = 18$ for $\text{BaCo}_3(\text{VO}_4)_2(\text{OH})_2$. Figures 5(b) and 5(c) show the magnetic contribution C_{mag}/T obtained by subtracting this lattice contribution from the experimental data and the magnetic entropy S_{mag} calculated by integrating the magnetic C_{mag}/T with respect to T assuming the C_{mag}/T -value equals 0 at 0 K following the third law of thermodynamics. The asymptotic value of S_{mag} at high temperatures close to $R \ln 2 = 5.76 \text{ mol}^{-1} \text{K}^{-1}$ expected for a doublet demonstrates that the $J_{\text{eff}} = 1/2$ doublet is realized.

As shown in Fig. 5(c), the C_{mag}/T data of $\text{BaCo}_3(\text{VO}_4)_2(\text{OH})_2$ shows a broad hump at $T_{\text{SRO}} \sim 15$ K higher than T_N , indicating a short-range ordering. This hump can also be seen in the unsubtracted C/T data [indicated by the blue arrow in Fig. 5(a)]. On the other hand, as shown in Fig. 5(b), the C_{mag}/T data for $\text{Co}_3\text{V}_2\text{O}_7(\text{OH})_2 \cdot 2\text{H}_2\text{O}$ shows no apparent hump. However, up to around 50 K, which is considerably higher than T_N , there is a finite C_{mag}/T that decays with increasing temperature, indicating the development of short-range order. Furthermore, the S_{mag} data at T_N reach approximately 20% and 12% for $\text{Co}_3\text{V}_2\text{O}_7(\text{OH})_2 \cdot 2\text{H}_2\text{O}$ and $\text{BaCo}_3(\text{VO}_4)_2(\text{OH})_2$, respectively. These observations indicate that the development of short-range magnetic correlations above T_N has released magnetic entropy. The difference in the presence/absence of a distinct hump structure in C_{mag}/T data associated with the short-range ordering probably depends on the difference in magnetic dimensionality derived from their crystal structures—the V_2O_7 polyanions bound to the kagome layer of $\text{Co}_3\text{V}_2\text{O}_7(\text{OH})_2 \cdot 2\text{H}_2\text{O}$ are tightly chemically bound to the neighboring kagome layer, whereas the VO_4 polyanions bound to the kagome layer of $\text{BaCo}_3(\text{VO}_4)_2(\text{OH})_2$ are isolated

from the neighboring kagome layer. Therefore, the magnetic dimensionality must be derived from the "built-in" character of a crystal structure, being consistent with the higher T_N and H_M in $\text{Co}_3\text{V}_2\text{O}_7(\text{OH})_2 \cdot 2\text{H}_2\text{O}$.

IV. Discussion

$\text{Co}_3\text{V}_2\text{O}_7(\text{OH})_2 \cdot 2\text{H}_2\text{O}$ and $\text{BaCo}_3(\text{VO}_4)_2(\text{OH})_2$ are Co^{2+} analogues of the kagome copper minerals volborthite and vesignieite. The observed effective magnetic moment, saturated magnetization, and magnetic entropy suggest a realization of $J_{\text{eff}} = 1/2$ doublet at low temperatures.

First, the observed metamagnetic-like transition with reduced M_0 is discussed. Both title materials exhibit $\sim 1/2 M_{\text{sat}}$ after metamagnetic-like transition, distinct from conventional metamagnets. Moreover, the maximum magnetization increases without saturation on increasing the applied magnetic field above H_M . The observed $M_{\text{sat}} \sim 2$ expected for $J_{\text{eff}} = 1/2$ probed by pulsed magnetization measurements demonstrates that the small M_0 is not due to temperature effects. This behavior is consistent with a noncollinear spin structure such as a canted antiferromagnetic order. In a noncollinear spin structure, spin canting creates an uncompensated net moment. The coplanar 120-degree spin structure is most stable without Dzyaloshinskii-Moriya (DM) interactions in the classical kagome-lattice antiferromagnets [43].

On the other hand, due to finite DM interactions, all spins tilt from the kagome plane to an umbrella-like structure, resulting in a spontaneous magnetization [44-46]. Essentially, there is no inversion center at the middle point of the coupling between neighboring magnetic sites in the kagome-lattice. Such magnetic structures have been universally observed in several jarosite-type materials [47,48] and rare-earth kagome $R_3\text{Sb}_3\text{Mg}_2\text{O}_{14}$ ($R = \text{Nd}, \text{Dy}$) [49,50]. Hence, spontaneous magnetization emerges within a single kagome layer. In this situation, a metamagnetic-like transition in which antiferromagnetically-aligned net moments in the layer change to ferromagnetically-aligned ones can emerge, as shown in Fig. 6. Such a metamagnetic-like transition of the net moment has been observed in jarosite-type $\text{AFe}_3(\text{OH})_6(\text{SO}_4)_2$ ($A = \text{K}, \text{Ag}$) [51,52].

Next, we discuss the magnitude of the single-layer net magnetization. The order of the \mathbf{D} vector can be estimated using the following equation [53,54],

$$|\mathbf{D}| \sim \frac{g - g_{\text{spin}}}{g} 2J \quad (5)$$

, where $g_{\text{spin}} (= 2)$ is the spin-only g -value, and J is the exchange interaction. The canting angle θ from the plane of coplanar spin structure with the competition and DM interactions as

$$\tan \theta = \frac{|\mathbf{D}|}{2J} \sim \frac{g - g_{\text{spin}}}{g}. \quad (6)$$

The expected in-plane spontaneous magnetization M_0 using the θ -value obtained with the experimentally observed $g \sim 4$ is calculated to be $M_0 \sim 0.45 M_{\text{sat}}$. Therefore, it is possible to

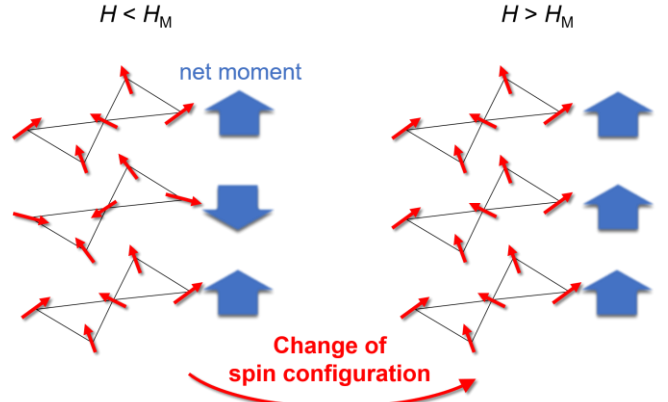


Fig. 6 Schematic view of the change of spin configuration in which the antiferromagnetically aligned canted moments changes to ferromagnetically aligned ones in $\text{Co}_3\text{V}_2\text{O}_7(\text{OH})_2 \cdot 2\text{H}_2\text{O}$ and $\text{BaCo}_3(\text{VO}_4)_2(\text{OH})_2$.

explain the observed reduced M_0 from the DM interaction alone in Co^{2+} ions. Note that the spontaneous magnetization of the field-induced phases is powder-averaged since the measurements were performed on powder samples. Thus, it is difficult to determine whether the reduced M_0 originates solely from DM interactions in the present stage. Therefore, the future establishment of single crystal growth will clarify the exact origin of the reduced M_0 . Moreover, the absence of the $1/3$ plateau characteristic of kagome-lattice antiferromagnets would be due to the in-plane net moment of $\sim 1/2 M_{\text{sat}}$ in canting spin structure transcending that of $1/3 M_{\text{sat}}$ in the up-up-down one. Neutron diffraction experiments are a future issue to clarify the details of these magnetic structures, and it is urgent to establish a synthetic method for deuterated title materials $\text{Co}_3\text{V}_2\text{O}_7(\text{OD})_2 \cdot 2\text{D}_2\text{O}$ and $\text{BaCo}_3(\text{VO}_4)_2(\text{OD})_2$.

Finally, we discuss the influence of DM interactions on magnetic susceptibility. By Moriya, an extended Curie-Weiss rule that incorporates the DM interaction by molecular field approximation has been given as follows,

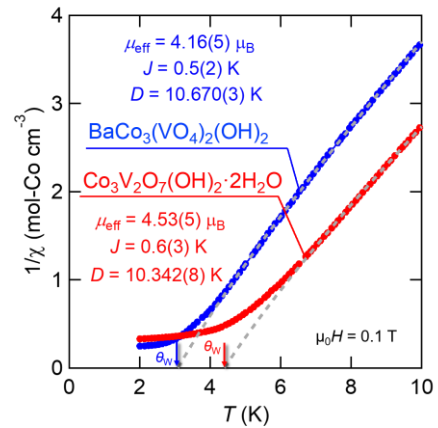


Fig. 7 Results of the modified Curie-Weiss fit incorporating the Dzyaloshinskii-Moriya interaction in the molecular field approximation to the $1/\chi$ data on the temperature dependence of the inverse susceptibility at low-temperature ($7 < T/\text{K} < 10$) regions.

$$\chi = \frac{N\mu_{\text{eff}}^2}{3k_{\text{B}}(T - \theta_{\text{w}})} \frac{(T + T_0)}{(T + \theta_{\text{w}})} + \chi_0, \quad (7)$$

with

$$\theta_{\text{w}} = \frac{JzS(S+1)}{3k_{\text{B}}} \left[1 + \left(\frac{|\mathbf{D}|}{J} \right)^2 \right]^{\frac{1}{2}}, \quad (8)$$

$$T_0 = \frac{JzS(S+1)}{3k_{\text{B}}}, \quad (9)$$

,where z indicates the coordination number; $z = 4$ in kagome lattice [54]. The results of the fitting using Eq. (7) for the $1/\chi$ data below 10 K are shown in Fig. 7. Here, to reduce fitting errors, χ_0 was fixed to the value of χ_{HV} estimated from the high-field magnetization process [see Fig. 4(f)]. The fits yield $\mu_{\text{eff}} = 4.53(5) \mu_{\text{B}}$, $J = 0.6(3) \text{ K}$, and $|\mathbf{D}| = 10.342(8) \text{ K}$ for $\text{Co}_3\text{V}_2\text{O}_7(\text{OH})_2 \cdot 2\text{H}_2\text{O}$, and $\mu_{\text{eff}} = 4.16(5) \mu_{\text{B}}$, $J = 0.5(2) \text{ K}$, and $|\mathbf{D}| = 10.670(3) \text{ K}$ for $\text{BaCo}_3(\text{VO}_4)_2(\text{OH})_2$. The thus-obtained θ_{w} -values, corresponding to the intercept of the T -axis, are 4.4 K and 3.0 K for $\text{Co}_3\text{V}_2\text{O}_7(\text{OH})_2 \cdot 2\text{H}_2\text{O}$ and $\text{BaCo}_3(\text{VO}_4)_2(\text{OH})_2$, respectively, roughly consistent with the magnetic transition temperatures T_{N} . These results indicate that relatively large DM interactions dominantly stabilize the magnetic order. Here, given the relationship in Eq. (5), it is mysterious that J is so small relative to $|\mathbf{D}|$, of which the reasonable origin is a cancellation of several competing superexchange interactions with different signs. For example, ferromagnetic Kitaev interactions expected for Co^{2+} magnets possibly compete with

conventional Heisenberg antiferromagnetic interactions [55,56]. In the present stage, extracting them independently from the magnetic susceptibility analysis is impossible. Therefore, inelastic neutron scattering experiments are planned to estimate the exchange parameters needed to construct reasonable spin models for $\text{Co}_3\text{V}_2\text{O}_7(\text{OH})_2 \cdot 2\text{H}_2\text{O}$ and $\text{BaCo}_3(\text{VO}_4)_2(\text{OH})_2$.

V. Summary

We have synthesized the high-quality polycrystalline samples of $\text{Co}_3\text{V}_2\text{O}_7(\text{OH})_2 \cdot 2\text{H}_2\text{O}$ and $\text{BaCo}_3(\text{VO}_4)_2(\text{OH})_2$ via a hydrothermal route and investigated their magnetism and thermodynamic properties. We have shown that they are promising model compounds for the $J_{\text{eff}} = 1/2$ kagome-lattice magnets. The observed canted ferromagnetic state with a halfway-saturated magnetic net moment originates from the DM interaction and the large g-factor, which would be characterized as an emblematic property of the $J_{\text{eff}} = 1/2$ kagome magnets. The $J_{\text{eff}} = 1/2$ kagome magnets will provide us with a unique platform to study quantum magnetism.

Acknowledgment

This work was supported by Japan Society for the Promotion of Science (JSPS) KAKENHI Grant Number JP22K14002, JP19K14646, and JP21K03441. Part of this work was carried out by joint research in the Institute for Solid State Physics, the University of Tokyo.

[1] L. Balents, *Nature (London)* 464, 199 (2010).
[2] L. Savary and L. Balents, *Rep. Prog. Phys.* 80, 016502 (2017).
[3] Y. Zhou, K. Kanoda, and T.-K. Ng, *Rev. Mod. Phys.* 89, 025003 (2017).
[4] C. Broholm, R. J. Cava, S. A. Kivelson, D. G. Nocera, M. R. Norman, and T. Senthil, *Science* 367, eaay0668 (2020).
[5] M. A. de Vries, J. R. Stewart, P. P. Deen, J. O. Piatek, G. J. Nilsen, H. M. Rönnow, and A. Harrison, *Phys. Rev. Lett.* 103, 237201 (2009).
[6] T.-H. Han, J. S. Helton, S. Chu, D. G. Nocera, J. A. Rodriguez-Rivera, C. Broholm, and Y. S. Lee, *Nature (London)* 492, 406 (2012).
[7] M. R. Norman, *Rev. Mod. Phys.* 88, 041002 (2016).
[8] M. A. de Vries, K. V. Kamenev, W. A. Kockelmann, J. Sanchez-Benitez, and A. Harrison, *Phys. Rev. Lett.* 100, 157205 (2008).
[9] A. Olariu, P. Mendels, F. Bert, F. Duc, J. C. Trombe, M. A. de Vries, and A. Harrison, *Phys. Rev. Lett.* 100, 087202 (2008).
[10] D. E. Freedman, T. H. Han, A. Prodi, P. Müller, Q.-Z. Huang, Y.-S. Chen, S. M. Webb, Y. S. Lee, T. M. McQueen, and D. G. Nocera, *J. Am. Chem. Soc.* 132, 16185 (2010).
[11] Z. Zhu, P. A. Maksimov, S. R. White, and A. L.

Chernyshev, *Phys. Rev. Lett.* 119, 157201 (2017).
[12] I. Kimchi, J. P. Sheckelton, T. M. McQueen, and P. A. Lee, *Nat. Commun.* 9, 4367 (2018).
[13] Z. Hiroi, M. Hanawa, N. Kobayashi, M. Nohara, H. Takagi, Y. Kato, and M. Takigawa, *J. Phys. Soc. Jpn.* 70, 3377 (2001).
[14] H. Yoshida, J. Yamaura, M. Isobe, Y. Okamoto, G. J. Nilsen, and Z. Hiroi, *Nat. Commun.* 3, 860 (2012).
[15] H. Ishikawa, M. Yoshida, K. Nawa, M. Jeong, S. Krämer, M. Horvatić, C. Berthier, M. Takigawa, M. Akaki, A. Miyake, M. Tokunaga, K. Kindo, J. Yamaura, Y. Okamoto, and Z. Hiroi, *Phys. Rev. Lett.* 114, 227202 (2015).
[16] Y. Okamoto, H. Yoshida, and Z. Hiroi, *J. Phys. Soc. Jpn.* 78, 033701 (2009).
[17] R. Okuma, T. Yajima, D. Nishio-Hamane, T. Okubo, and Z. Hiroi, *Phys. Rev. B* 95, 094427 (2017).
[18] R. Okuma, D. Nakamura, T. Okubo, A. Miyake, A. Matsuo, K. Kindo, M. Tokunaga, N. Kawashima, S. Takeyama, and Z. Hiroi, *Nat. Commun.* 10, 1229 (2019).
[19] M. Goto, H. Ueda, C. Michioka, A. Matsuo, K. Kindo, and K. Yoshimura, *Phys. Rev. B* 94, 104432 (2016).
[20] R. Shirakami, H. Ueda, H. O. Jeschke, H. Nakano, S. Kobayashi, A. Matsuo, T. Sakai, N. Katayama, H. Sawa, K. Kindo, C. Michioka, and K. Yoshimura, *Phys. Rev. B* 100,

- 174401 (2019).
- [21] A. Abragam and M. H. L. Pryce, Proc. R. Soc. A 206, 173 (1951).
- [22] M. E. Lines, Phys. Rev. 131, 546 (1963).
- [23] H. Shiba, Y. Ueda, K. Okunishi, S. Kimura, and K. Kindo, J. Phys. Soc. Jpn. 72, 2326 (2003).
- [24] O. Kahn, *Molecular Magnetism* (Wiley-VCH, Weinheim, 1993).
- [25] F. Lloret, M. Julve, J. Cano, R. Ruiz-García, and E. Pardo, Inorg. Chem. Acta 361, 3432 (2008).
- [26] M. Fujihala, X. G. Zheng, Y. Oohara, H. Morodomi, T. Kawae, A. Matsuo, and K. Kindo, Phys. Rev. B 85, 012402 (2012).
- [27] T. Đorđević, L. Karanović, Acta Crystallogr., Sect. C: Struct. Chem. 69, 114–118 (2013).
- [28] S. B. Ni, T. Li, X. L. Yang, Mater. Lett. 65 2662-2664 (2011).
- [29] S. Zhang, H. Yun, H. Yu, J. Alloys Compd. 735, 700, (2018)
- [30] R. Dessapt, L. Lajaunie, J. J. Calvino, P. Deniard, I. Trenquea and C. Payen, J. Mater. Chem. C 10, 3287 (2022)
- [31] K. Momma and F. Izumi, J. Appl. Crystallogr. 44, 1272 (2011).
- [32] F. Izumi, and K. Momma, Solid State Phenom. 130, 15 (2007).
- [33] S. K. Banerjee, Phys. Lett. 12 16 (1964)
- [34] P. F. Bongers, C. F. van Bruggen, J. Koopstra, W. P. F. A. M. Omloo, G. A. Wiegers, and F. Jellinek, J. Phys. Chem. Solids 29, 977 (1968)
- [35] B. Huang, G. Clark, E. Navarro-Moratalla, D. R. Klein, R. Cheng, K. L. Seyler, D. Zhong, E. Schmidgall, M. A. McGuire, D. H. Cobden et al., Nature (London) 546, 270 (2017).
- [36] J. Wang, J. Deng, X. Liang, G. Gao, T. Ying, S. Tian, H. Lei, Y. Song, X. Chen, J. Guo, X. Chen, Phys. Rev. Materials 5 (2021) L091401.
- [37] J. Yang, B. Chen, H. Wang, Q. Mao, M. Imai, K. Yoshimura, and M. Fang, Phys. Rev. B 88 (2013) 064406.
- [38] S. Kobayashi, H. Ueda, C. Michioka, and K. Yoshimura, Inorg. Chem. 55, 7407 (2016).
- [39] A. Arrott, Phys. Rev. 108, 1394 (1957).
- [40] A. R. Kampf, I. M. Steele Can. Mineral., 46, 687–692 (2008).
- [41] See Supplemental Material at [URL will be inserted by publisher] for the heat capacity data of $\text{Zn}_3\text{V}_2\text{O}_7(\text{OH})_2 \cdot 2\text{H}_2\text{O}$ for comparison.
- [42] P. Svoboda, P. Javorský, M. Diviš, V. Sechovský, F. Honda, G. Oomi, and A. A. Menovsky, Phys. Rev. B 63, 212408 (2001).
- [43] A. B. Harris, C. Kallin, and A. J. Berlinsky, Phys. Rev. B 45, 2899 (1992).
- [44] M. Elhajal, B. Canals, and C. Lacroix, Phys. Rev. B 66, 014422 (2002).
- [45] M. Elhajal, B. Canals, and C. Lacroix, Physica B 312, 716 (2002).
- [46] R. Ballou, B. Canals, M. Elhajal, C. Lacroix, and A. S. Wills, J. Magn. Magn. Mater. 262, 465 (2003).
- [47] S.-H. Lee, C. Broholm, M. F. Collins, L. Heller, A. P. Ramirez, Ch. Kloc, E. Bucher, R. W. Erwin, and N. Lacey, Phys. Rev. B 56, 8091 (1997).
- [48] T. Morimoto, M. Nishiyama, S. Maegawa, and Y. Oka, J. Phys. Soc. Jpn. 72, 2085 (2003).
- [49] A. Scheie, M. Sanders, J. Krizan, Y. Qiu, R. J. Cava, and C. Broholm, Phys. Rev. B 93, 180407(R) (2016).
- [50] J. A. M. Paddison, H. S. Ong, J. O. Hamp, P. Mukherjee, X. Bai, M. G. Tucker, N. P. Butch, C. Castelnovo, M. Mourigal, and S. E. Dutton, Nat. Commun. 7, 13842 (2016).
- [51] D. Grohol, K. Matan, J. H. Cho, S. H. Lee, J. W. Lynn, D. G. Nocera, and Y. S. Lee, Nature Mater. 4, 323 (2005).
- [52] K. Matan, B. M. Bartlett, J. S. Helton, V. Sikolenko, S. Matas, K. Prokes, Y. Chen, J. W. Lynn, D. Grohol, T. J. Sato, M. Tokunaga, D. G. Nocera, and Y. S. Lee, Phys. Rev. B 83, 214406 (2011).
- [53] I. E. Dzyaloshinskii, J. Phys. Chem. Solids 4, 241 (1958).
- [54] T. Moriya, Phys. Rev. 120, 91 (1960).
- [55] H. Liu, J. Chaloupka, and G. Khaliullin, Phys. Rev. Lett. **125**, 047201 (2020).
- [56] R. Sano, Y. Kato, and Y. Motome, Phys. Rev. B 97, 014408 (2018).

Supplemental material for “Perfect kagome-lattice antiferromagnets with $J_{\text{eff}} = 1/2$: The Co^{2+} -analogs of copper minerals volborthite and vesignieite”

Yuya Haraguchi^{1,†}, Takehiro Ohnoda¹, Akira Matsuo², Koichi Kindo², and Hiroko Aruga Katori¹

¹Department of Applied Physics and Chemical Engineering, Tokyo University of Agriculture and Technology, Koganei, Tokyo 184-8588, Japan

²The Institute for Solid State Physics, The University of Tokyo, Kashiwa, Chiba 277-8581, Japan

†chiyuya3@go.tuat.ac.jp

In order to estimate the lattice contribution of heat capacity in $\text{Co}_3\text{V}_2\text{O}_7(\text{OH})_2 \cdot 2\text{H}_2\text{O}$, we measured the heat of $\text{Zn}_3\text{V}_2\text{O}_7(\text{OH})_2 \cdot 2\text{H}_2\text{O}$ (natural mineral Martyite), in which a nonmagnetic Zn ion substitutes the Co site of $\text{Co}_3\text{V}_2\text{O}_7(\text{OH})_2 \cdot 2\text{H}_2\text{O}$. Figure S1 shows the heat capacity of $\text{Zn}_3\text{V}_2\text{O}_7(\text{OH})_2 \cdot 2\text{H}_2\text{O}$. For comparison, the specific heat data of $\text{Co}_3\text{V}_2\text{O}_7(\text{OH})_2 \cdot 2\text{H}_2\text{O}$ (the same as in the text) and the calculated phonon contribution are also included. The C/T data for both materials do not agree over the entire temperature range, and especially not at all good agreement is obtained in the high-temperature range. The origin of this discrepancy is probably due to the difference in lattice vibrations caused by the different strength of the local chemical bonds between transition metal ions and oxygen ions in Co and Zn, although the two materials are structurally very similar. Hence, $\text{Zn}_3\text{V}_2\text{O}_7(\text{OH})_2 \cdot 2\text{H}_2\text{O}$ is not a suitable nonmagnetic reference material for estimating the lattice-specific heat in $\text{Co}_3\text{V}_2\text{O}_7(\text{OH})_2 \cdot 2\text{H}_2\text{O}$.

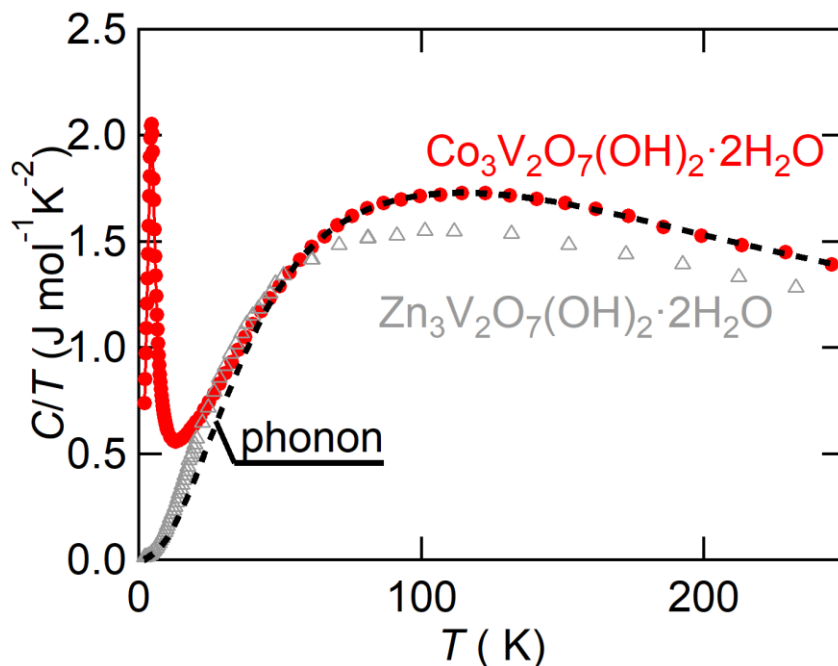


Fig. S1. The temperature dependence of $\text{Co}_3\text{V}_2\text{O}_7(\text{OH})_2 \cdot 2\text{H}_2\text{O}$ and $\text{Zn}_3\text{V}_2\text{O}_7(\text{OH})_2 \cdot 2\text{H}_2\text{O}$. The calculated phonon contribution in $\text{Co}_3\text{V}_2\text{O}_7(\text{OH})_2 \cdot 2\text{H}_2\text{O}$ is also displayed (See the main text for calculation method).